"Drone-based persistent surveillance system on large circular perimeters: Design and Performance Assessment"

This paper investigates the use of a homogeneous fleet of drones for fully-automated cyclic patrolling a vast circular perimeter, supported by auxiliary on-ground charging stations wherein the drones land and automatically recharge without human intervention. We firstly present a non-linear MILP model for defining a cyclic schedule of flight missions – with non-coincident start (take-off) and end (landing) locations – that we aim at the minimization of both, coverage time and fleet size. Its resolution provides the drone platform to use for revisiting each of the sectors in which we split the perimeter, along with the location of each base station and a number of drones at each one. We secondly propose a DES model incorporating the accelerated depletion of Li-Po batteries as an uncertainty source effecting on real-life flight times. Based on our computational experiments, both, the fleet size and the sectors partitioning effect the robustness of the system.

Keywords: multidrone persistent guarding perimeter operation, automatic battery recharging technology, non-linear MILP, discrete event simulation, robust circular perimeter patrolling schedules.

1. Introduction

Persistent aerial surveillance around unmanned aerial systems (UAVs) is a routine operation in many Intelligence, Surveillance and Reconnaissance (ISR) missions. Examples of applications (Nigam, 2014) include both military and civil applications such as detecting illegal ground activities (Dempsey, 2014), maritime surveillance (Fauske et al., 2020) or the provision of coverage and connectivity to ground users and first responders in emergency situations (Shi et al., 2018). Typically, such applications are aimed at ensuring that the maximum amount of information is gathered, oftentimes over a large area and during a long time.

Influenced by the rapid development of technology, UAVs are more and more introduced as a part of technical equipment for security work. For instance, the security work around UAVs is nowadays fully usable in protecting railway and transport hubs, in order to detect and limit different types of incidents which otherwise would adversely impact the integrity and availability of their sites and systems (Sărăcin et al., 2017). Instead of deploying security cameras around the areas to cover and having security staff patrol, the

authorities can plan the real-time monitoring of various sites benefiting from drones mobility and cost-effectiveness.

In this paper, we cope with the practical situation in which a fleet of homogeneous UAVs is to be set in automatic mode for persistently patrolling a vast circular perimeter surrounding a critical security area. Our assumption on the used drones does not suppose any complex UAV engineering: it is compatible with today's professional drones with features like waypoint navigation and trajectory following using Global Positioning System (GPS). However, we deep on the automation of the system by considering that we settle a variety of on-ground replenishment stations – several conceptions appeared in recent years (Fetisov & Akhmerov, 2019; Nguyen et al., 2020) -, where the drones land and automatically recharge without any human intervention. Although the deployment of this infrastructure leads to certain initial cost – e.g. we refer the reader to the commercial solution at www.skycharge.de -, it is insignificant as compared to the reduction in operational costs from avoiding the need for workers/guards patrolling the perimeter.

Our research approach is mainly concerned on conceptualizing the system according to a list of practical considerations. Firstly, we assume that UAVs transmit live video feed to control rooms on-ground, what is supported by means of installed communication receivers at the same locations wherein the charging stations are installed. Henceforth, these points will be referred as base stations. There are practical reasons to avoid their placement too close to the perimeter: *(i)* Avoiding the need of extending the power line required to feed the charging ground stations too far from the centre of the critical area, and *(ii)* Limiting the risk of vandalism when setting these kind of infrastructures too close to the perimeter. Secondly, our collection of data is not only serving the purpose of providing the security staff with the real-time visualization of the received images being perceived by the guarding UAVs – for instance using a first person view system as in Saha et al. (2017)-, but also of benefiting from the possibilities of current photogrammetry techniques on the aerial images gathered while patrolling the perimeter. For instance, once a fencing breach was identified, a high-resolution scene reconstruction can be created from the gathered images.

Our studied application is a particular case of the continuous monitoring problem (CMP), where the main decision is how splitting our vast circular perimeter into sections on which scheduling periodic photogrammetry patrolling (at a fixed and typically low velocity)

missions in such a manner that every point in the perimeter is revisited with a limited span time. Aside from the patrolling frequency, operational constraints such as communication limitations, practical conditions on the placement of base stations and time of recharging (among others) are considered. Briefly, we have developed a non-linear mixed integer-linear programming (MILP) model as an optimization approach for defining the cyclic schedule of the flight missions. For instance, Fig. 1 depicts one of such cyclic patterns: the circular perimeter is split into 8 sections and 16 drones (every arrow) are required to be flying at the same. As will be explained later, this means that each drone's flight mission will serve two of the eight portions in which the circle perimeter is split.

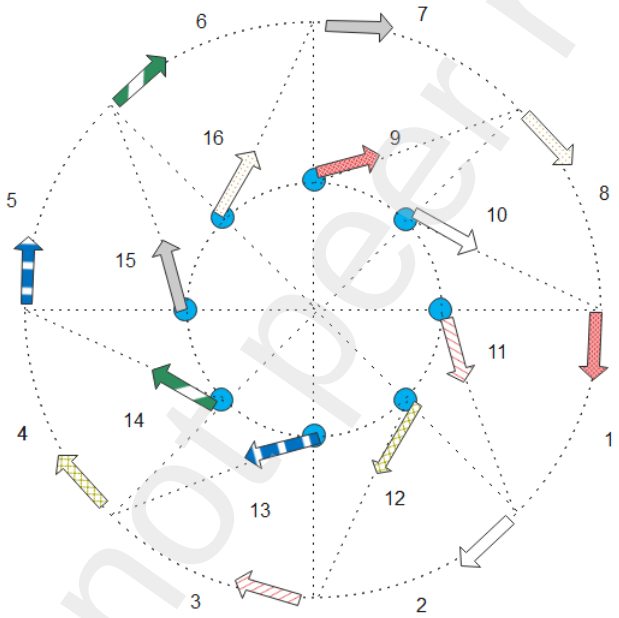

Fig. 1. Example where the required regular patrolling of the circular perimeter is based on a swarm of 16 drones (arrows) flying at the same time and a set of eight base stations (circles). Notice we indicate the source base station for every drone –e.g. the base station from which the 16th drone is taking-off is the same from which the 8th drone formerly took-off.

While the traditional CMP is aimed at maximizing the visiting frequency of targets (Mersheeva & Friedrich, 2015; Kim & Morrison, 2014), we aim our optimization model at the minimization of both, revisiting time and fleet size. On solving the MILP we are deciding:

- The size of the fleet of homogeneous drones and the mobility pattern for each member in the fleet. Namely, the agenda and schedule for each UAV in terms of how and when it travels over the perimeter –i.e. serve a portion of the perimeter and go to the base station to start its battery replenishment process.
- The quantity and placement of base stations that, aside from acting as control stations that monitors the flight missions and replenishment stations, are also static depots from which the already replenished UAVs take-off.
- The time between revisits (the inverse of the patrolling frequency performed) and the value of the cruise velocity used when approaching and leaving the perimeter.
- The selected platform, from the short-listed candidate commercial UAVs under consideration.

As it is the case of the large majority of today's off-the-shelf inexpensive UAVs, we assume the drone platform to be vertical take-off and landing (VTOL) with brushless electro-motors powered by rechargeable Lithium-ion Polymer (Li-Po) batteries, which are lighter-weight and higher capacity (providing a higher specific energy) than their counterparts (Boggio-Dandry & Soyata, 2018). It is worth commenting that such vehicles are capable of travelling at a constant speed between a pair of locations, and whilst windy conditions may impact the actual speed attained, there are ways to adjust the thrust during the journey to maintain a stable speed. A downside of this is that it introduces uncertainty in the battery lifetime, which is in fact a major concern for the robustness of the operational design of our drone-based surveillance system.

Considering that we are in the design stage of the system, major attention has been paid to the realistic exploitation of the cyclic pattern provided by the MILP resolution. To this aim, we have developed a discrete-event simulation (DES) model that considers the power drained as a function of flight velocity (fixed by the MILP solution, except for the patrolling velocity which, by design, is selected beforehand), whereas introduces random occurrences of accelerated depletion of batteries to check the extent to which a certain fleet size is robust against the effect of uncertainty on flight times. In short, we propose ultimately deciding the operational design of our persistent surveillance system only once the robustness of the fleet size is assessed and validated –i.e., there is evidence on the sufficient protection attained against the effect of uncertainty on the flight times.

The remainder of the paper is as follows. Section 2 revises the literature. Section 3 presents the description of our problem and contains the non-linear MILP formulation; Section 4 details the DES developed to find the fleet required for attaining a robust performance of our circular perimeter patrolling system. Section 5 contains the set of experiments designed to assess the validity of the adopted approach, wherein the effect due to the different parameters (both, at the first stage around the MILP and at the second stage around the DES) is analysed. Finally, Section 6 is devoted to conclusions and further research lines.

2. Literature Review

The problem under study is within the category "routing for a set of locations" (Otto et al., 2018), since we aimed at finding the optimal routes for the vehicles in the system to achieve a given objective –namely, a trade-off between the pursued fleet size minimization and the span of the revisits to the perimeter.

In this section, we first discuss routing papers that are directly relevant to our optimization approach for defining the cyclic schedule of a fleet of vehicles, and then we revise the literature concerning the lifetime of the electrical batteries in use at these vehicles.

2.1. Routing a set of locations

The design approach for setting up a continuous monitoring system on a fleet of UAVs for the surveillance of our vast perimeter exhibits similarities with former literature. Burdakov et al. (2017) have recently considered the problem of replacing security UAVs performing a surveillance mission along a perimeter. The authors determined which UAV to replace and when, while minimizing the effect this had on the chances of observing an intruder attempting to penetrate the perimeter. Their assumption of spare UAVs available and on stand-by to replace UAVs whose batteries are low is also in Hartuv et al. (2018) and Park & Morrison (2019). Hartuv et al. (2018) minimized the number of UAVs to be used when the replacement point was the single depot from which the UAVs are launched, whereas Park & Morrison (2019) did it around multiple replacement stations. In contrast with the former studies, other researchers (Drucker et al., 2016; Ho & Ouaknine, 2015) have also sought to find a cyclic schedule of missions on a set of points of interest so that everyone is repeatedly visited by some UAV at intervals of duration bounded by an every

point-dependent deadline. Ho & Ouaknine (2015) shown there was no polynomial bound on the solution route, whereas Drucker et al. (2016) were focused on finding the number of UAVs required and their cyclic routes assuming they start and end at the same vertex and can visit vertices multiple times. However, what is needed in our studied surveillance application is a cyclic schedule of the flight missions but with non-coincident start (take-off) and end (landing) points.

As reported in recent logistics literature (Li et al., 2018), allowing the route of a vehicle to start from a depot and end at any other of the depots can potentially reduce delivery distance and fuel/energy consumption because more choices are provided for route arrangement. Li et al. (2018) presented the benefits of this strategy for the e-commerce logistics operation in big urban areas when the serving vehicle is not required to return to the depot from which it started, since an information system allows for the flexible matching of the incoming Internet orders with the real-time knowledge of drivers' and vehicles' position.

Another strategy to gain flexibility consists of transiting for intermediate facilities others than the one the vehicle starts (Schneider et al., 2015; Crevier et al., 2007 ; Angelelli & Speranza, 2002). The insertion of intermediate stops in the route has been considered in Schneider et al. (2015) for planning electric vehicle routing problems with recharging facilities, therein charging times based on the remaining battery charge. Crevier et al. (2007) addressed a real-life grocery distribution problem wherein the route of a truck can be composed of multiple stops at intermediate depots where the vehicle has to be replenished. The replenishment at intermediate facilities has also been considered in Angelelli & Speranza (2002) as an extension of the periodic VRP (PVRP) where the vehicles can renew their capacity at some intermediate facilities. Since the goal in our design approach is defining the persistent continuous (non-stop) monitoring service with recharging events and periodic visits to points, our case study could be viewed as a particular case of a PVRP wherein the period is the time needed for the full coverage of the set of points. Nevertheless, the straightforward application of PVRP modelling would lead us to impose that, at each period, every vehicle detours to return to its base (Cordeau et al., 1997), and definitely this does not allow us for the flexibility required on modelling our case study.

Recently, Mersheeva & Friedrich (2015) have addressed the UAV-based CMP with inter-depot routes to account for supporting sites wherein drones can renew their energy. They calculate a sequence of routes for every UAV in order to maximize the number of visits to the points of interest, thereby minimizing the delays between the visits during a given planning horizon. While human intervention was still needed for accomplishing the batteries replacement at the supporting stations in their approach, in our studied problem it was not: an UAV with low-level batteries lands at one of the ground charging stations based on open contact pads and automatically recharges without any human intervention.

2.2. Li-Po batteries and flight time

The practical discharge duration of a Li-Po battery is dependent on a sort of factors (from the environmental temperature to the number of charging/discharging cycles), and has been investigated around different constant power rates (Nebl et al., 2020) to conclude that the linear energy/power Peukert's law (which describes the correlation between discharge current and discharge duration) is no longer valid any upon the application of high constant power (namely, at power loads above the specifications of the cells). However, the reported UAV's applications have in fact neglected this dynamic behaviour of their batteries energy storage.

The classical power consumption models for electrical UAVs have combined the basic equations of flight dynamics and translated them into the electrical domain, based mostly on the specifications given from cells manufacturers along with the precise knowledge of the payload (namely, weight and energy drainage due to the on-board sensors). However, according to Zhang et al. (2021), "…flight distances and energy consumption are likely to be inaccurate when based on flight times and speeds reported by manufacturers that are either maximum values or from unknown operating conditions". Zhang et al. (2021) identify key factors that affect drone energy consumption and discuss similarities and differences among various models. For cruising flight, drone power consumption can be modelled as a convex function of a drone's total weight e.g., (Kirschstein, 2020; Liu et al., 2017; Stolaroff et al., 2018), while for hovering it is proportional to the weight to the power 1.5 (Dorling et al., 2017). Notice that in our case study no delivery is involved (no effect of weight changes needs to be incorporated) and consumptions are mainly due to cruising horizontal flights.

Among the prior research works that considers the electrical power consumption as a function of the UAV cruise velocity we can refer to the works by D'Andrea (2014), Dukkanci et al. (2021), Zeng et al. (2019) and Zhang et al. (2021). D'Andrea (2014) approximated the power consumption of such flights as a linear function of velocity once fixed the lift-to-drag ratio (which encompasses aerodynamic and drone design aspects) and the power transfer efficiency (percentage of battery energy that we are transferring to motors and propellers). Zhang et al. (2021) studied the propeller power consumption as a function of the UAV speed when comparing five fundamental models for drone energy consumption of steady level flight (using the next values: batteries energy: 540J/kg, transfer efficiency from the battery to the propeller power: 70%, safety factor to reserve energy in the battery for unusual conditions: 80%). Zeng et al. (2019) also analysed the profile of power as a function of velocity to further claiming that there are two practical velocities of interest: that providing maximal endurance (or time) and that providing maximal range (or distance). Dukkanci et al. (2021) followed the non-linear power consumption model in Zeng et al. (2019) to decide the speed of the UAV in a drone delivery problem.

Besides, since it is well-known that for maximizing Li-Po battery lifetime and efficiency it is not recommended that the depth of discharge exceeds 70-80%, there are several practical approaches to the energy-aware UAV displacement modelling that propose using safety factors when planning real-life UAV flight missions. Troudi et al. (2018) assumed an 80% of the energy; Stolaroff et al. (2018) considered a safety factor of 1.2 to reserve energy for unusual conditions (which is equivalent to using 83.3% of maximum flight distance). Figliozzi (2017) assumed that the drone flight range was only a 70% of the maximum flight distance to account for unknown factors (e.g., bad weather), thereby applying a safety margin to accommodate an eventual increase of energy consumption.

Noticeably, all the above works on the power consumption of electrical UAVs have in fact neglected the dynamic behaviour of their energy storage. Namely, they solely have combined the basic equations of flight dynamics and translate them into the electrical domain. However, inaccurate energy estimations arise from the assumption of the 1:1 correspondence between the power drawn by the electrical motor and the power decrease observed at the battery, since a battery supplies power depends on the amount of requested power.

The quicker than expected depletion of battery has been recently studied by Chen et al. (2019), concluding that the current power consumption models that attempt to combine the basic equations of flight dynamics and translate them into the electrical domain provided inaccurate energy estimations. The author suggested a non-linear shape dependent on the amount of requested power to model the efficiency of such a transformation. Importantly, since their approach captures the practical state-of-charge vs. time pattern under the typical current pulses required in electrical UAV missions, it can be referred to as battery-aware model. In practice, it allows for a better estimation of the point of accelerated depletion of batteries, forecasting lower flight times than those arising from the not battery-aware models.

From the previous literature review, we can conclude that, to the best of our knowledge, our drone-based persistent surveillance system on large circular perimeters is a novel problem and that on addressing it we need to study how to protect its performance from the effect of the uncertain flight times.

Next, we present a non-linear MILP model as an optimization approach for defining the cyclic schedule of flight missions – with non-coincident start (take-off) and end (landing) locations- that we aim at the minimization of both, coverage time and fleet size, to team the different UAVs up while considering the operational influence of electrical batteries two-fold. Firstly, we consider flight times using a safety factor to reserve energy in the battery (both, for caring Li-Po units and for accounting for the appearance of unusual conditions). Secondly, we incorporate the time requirements of recharging procedures at fixed points (Burdakov et al., 2017) – conversely to the non-fixed recharging locations reported in other practical scenarios (Gonzalez-R et al., 2020; Mathew et al., 2015). Aside from the limited endurance/flight time, the lengthy recharging time of the batteries is the other main factor influencing the number and locations of the fixed recharging stations needed. This factor complicates the planning of the UAV fleet, which is turned into deciding how best to schedule the corresponding replacements of patrolling UAVs for maintaining complete surveillance of the perimeter.

3. Problem Description and MILP formulation

In this section, we firstly derive the equations that, for a given drone platform and the practical considerations on its communications equipment, velocity range and endurance

constraints, relates: *(i)* the number of sectors in which we split the circular perimeter, *(ii)* the placement of the base stations and, *(iii)* the number of such drones that need to be part of the fleet. We then extend such a reasoning to the case where we are opened to select among a variety of drone platforms that would be used for the final provision of the persistent surveillance of the circular perimeter under design.

3.1. Definition of the mobility pattern on a given drone platform

Consider a circular perimeter (let's say a fence protecting a critical area) of radius R, wherein we consider the critical assets mostly concentrated in the centre of the area (particularly the Monitoring, Supervision & Control Centre which must receive and process the video surveillance images received by its communications antennas).

Aside from transmiting live video feed to the Control Centre, each UAV gathers images that ultimately will be input to a photogrammetry processing software for the high-resolution reconstruction of the recorded scenes. According to the camera on board, the required foot-print on the terrain leads us to set the UAV's flight at a constant height h. A typical requirement from the photogrammetry procedure concerns to the percentage of interleaving needed between successive perceived images that, along with the constant height h determines a fixed velocity V^{patrol} at which the aerial vehicle should track the perimeter. In our case, this value will be set to $V^{patrol} = 2\ m/s$. On the contrary, the cruise velocity on moving to or returning from the perimeter V^{cruise} is a decision variable.

In Fig. 2 we illustrate a single flight route for one of the guarding UAVs, which patrols a portion of the perimeter circumference of radius R, flying at a constant height h and continuously sending the video surveillance images to a base station settled at a radius $r \leq r_{max}$ (a limit that is imposed for practical reasons regarding power infrastructure and risk of vandalism on the replenishment stations).

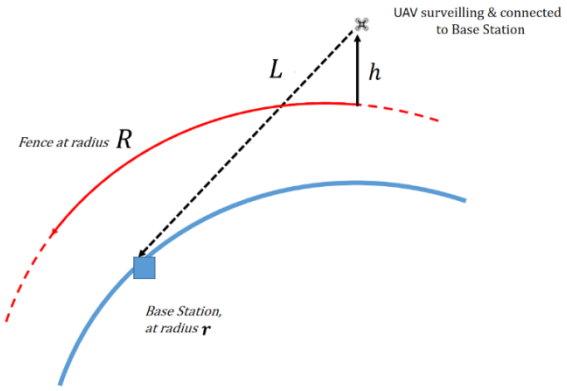

Fig. 2. The UAV patrolling the circle of radius R are linked to a base station settled at distance r. The distance between them should be within the range of the communications systems, L, for being able to continuously send the video surveillance images.

Individual UAVs have a restricted communications range and a maximal flight time, both limiting their effectiveness in the persistent surveillance application on the vast circular perimeter which motivates our research. However, we have devised a manner in which a fleet of homogeneous UAVs can be operated in automated mode and teamed up for overcoming these limitations and scale surveillance to the whole perimeter.

We propose a set of UAVs functioning as a distributed system. According to the illustrative example in Fig. 1, a swarm of drones will be flying at the same time so major attention is needed to precisely coordinating their behaviour. In Fig. 3 we present one of such flight missions, wherein an UAV (a) takes off from a base station, (b) approaches the fence in an oblique flight), as a practical way of avoiding collisions with a returning UAV following the shorter radial trajectory – i.e., being prepared for the quicker arrival at a safe point in the event of drained batteries-, (c) Patrols the perimeter and (d) Returns to land at a different base station before its maximal flight time or Endurance *E*.

It should be note that the health&security of the control communications is crucial in the monitoring of each automatic drone flight. As depicted in Fig. 3, along a typical drone's flight the communications control is handed over successive base stations, which for a while share the link to the aircraft. This is applied for reliability reasons, and only till the handover ultimately occurs when the UAV is just passing in front of the new commanding base station – e.g. in the example in Fig. 3, the base station at Q_0 will pass the control to the one at Q_1 once the UAV is at point P_1.

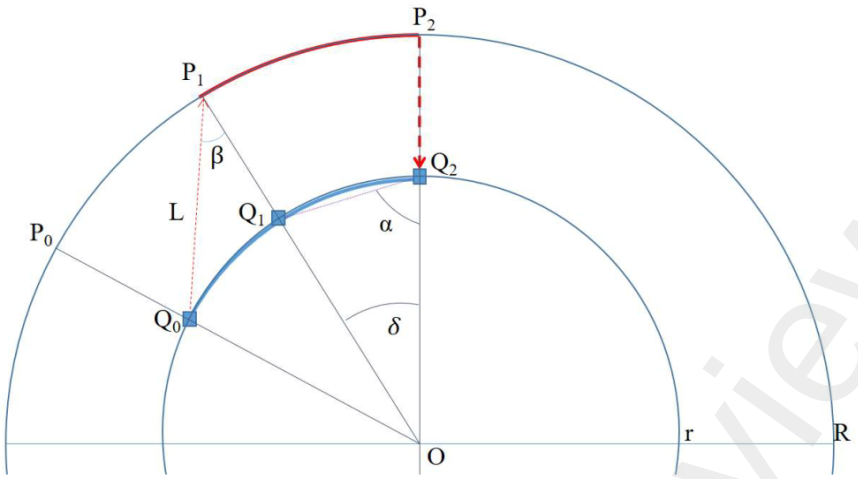

Fig. 3. The point for handing over the control of a UAV patrolling mission (P_1) must be still connected to its source base station Q_0. Beyond this, the control will be transferred to the base station at Q_1.

On the assumption that the base stations are equally distributed under the inner circle of radius r, we need to ensure that the maximal range for the in-use communications d_{max} is not exceeded. We next reduce our analysis on the accomplishment of this communication constraint to a 2D study, since we are interested in relatively large scenarios wherein the circle radius is of the order of thousands of meters whereas the value of the height h is quite small (practical values of $h = 30m$).

3.1.1 Range of communications and the Sectorization

We can relate the range of communications and the angle of each sector in which we are splitting the circle, δ, using the following trigonometry analysis.

In Fig. 3, a full drone's flight comprised of the segments Q_0-P_1, P_1-P_2 and P_2 -Q_2, serves the purpose of relating the length of the communication segment, denoted L, and the angle β wherein the hand-over from a base station to the next one occurs.

We can solve the triangle O-Q_0-P_1 to obtain

$$r^2 = L^2 + R^2 - 2LR\cos\beta \qquad (1)$$

Since the length of segment Q_1-P_2 is similar to that of segment Q_0-P_1, we can apply again the cosine theorem to resolve the triangle Q_0-Q_1-P_1 to express such length as:

$$(S^{Q0Q1})^2 = (R-r)^2 + L^2 - 2(R-r)\cdot L\cdot \cos\beta \quad (2)$$

We can substitute the term $2L\cdot\cos\beta$ deduced from Eq. (1) into Eq. (2) to get:

$$(S^{Q0Q1})^2 = (R-r)^2 + L^2 - (R-r)\cdot\left[\frac{L^2+R^2-r^2}{R}\right] \quad (3)$$

and from it, we can simplify to obtain the following expression for the distance till the hand-over point projection on the inner circle:

$$(S^{Q0Q1})^2 = \frac{r}{R}[L^2-(R-r)^2] \quad (3')$$

However, we can compute the same Euclidean distance according to the angle δ as $S^{Q0Q1} = 2r\sin\frac{\delta}{2}$, which once substitute in the former, leads to:

$$L^2 = 4Rr\cdot\sin^2\left(\frac{\delta}{2}\right) + (R-r)^2 \quad (4)$$

We finally can bound the length of this communications link at the maximal range of the access link from the base stations, d_{max}, as follows:

$$L \le d_{max} \quad (5)$$

3.1.2 Revisit time and velocity adjustments

Since the goal is patrolling the circular perimeter so that long time spans between revisits, the revisit time T^r has to be lower than the maximum allowed time MRT:

$$T^r \le MRT \quad (6)$$

For the sake of usability, the whole perimeter will be split into an integer number of sectors, S as follows:

$$S \cdot \delta = 2\pi \tag{7}$$

The whole perimeter comprises of $2\pi R$ meters to be patrolled at a fixed velocity V_{patrol}, from which the time T^r and the angle of each sector δ are related as follows:

$$T^r = \frac{R \cdot \delta}{V^{patrol}} \tag{8}$$

Aside from deciding the number of base stations (one for every sector, i.e., S), we have to establish the number of sectors n that are going to be patrolled by every mission flight. For instance, in Fig. 4 we sketch one example in which there are $n = 2$ sectors served by any single UAV mission flight.

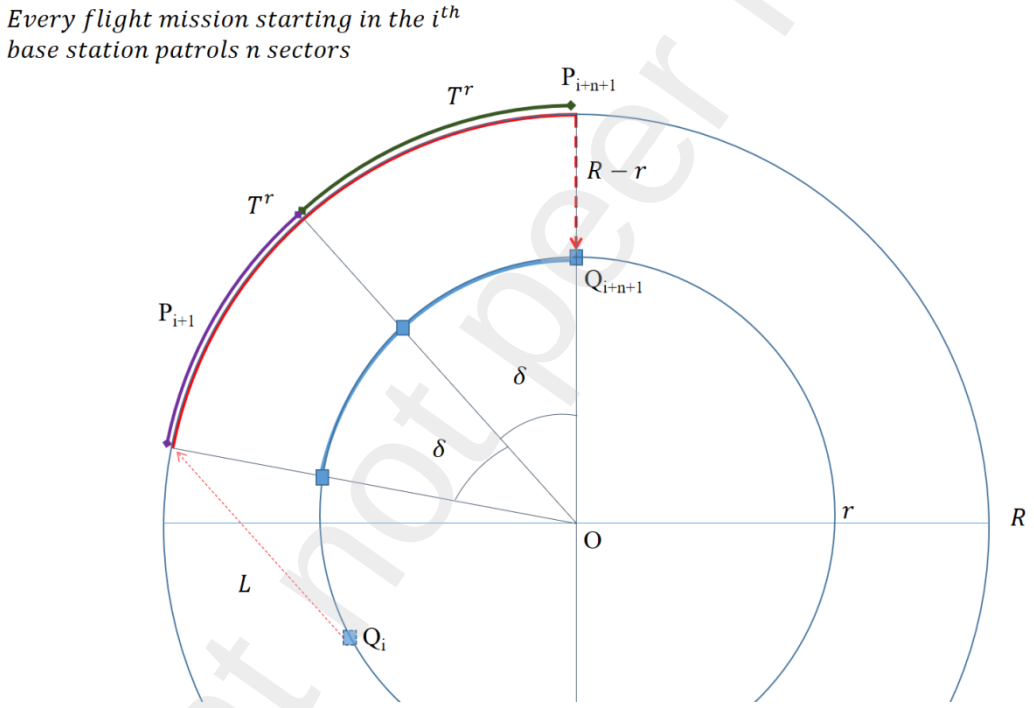

Fig. 4. Example of a guarding system configuration splitting the circle into S=9 sections, with single flights that are capable of guarding $n = 2$ consecutive perimeter parts.

Deciding on n highly depends on the commercial UAV models that we are considering as candidates to be the basis for our homogeneous fleet. To begin with, the manufacturer uses to publish an Endurance or maximal flight time, E , that we can relate to the number of sectors served by a single UAV flight n and the revisit time T^r as follows:

$$\frac{(R-r)}{V^{cruise}} + n \cdot T^{r} + \frac{L}{V^{cruise}} \leq E \quad (9)$$

Similarly, the manufacturer typically indicates the range of valid speeds:

$$MinSpeed \leq V^{cruise} \leq MaxSpeed \quad (10)$$

3.1.3 Safety margin on the Battery Energy Used

The overwhelming majority of commercial drones available today employ rechargeable Li-Po batteries, each Li-Po battery cell with a nominal voltage of 2.4 V, which are typically connected in series to attain a higher voltage. Importantly, when the depth of discharge (DOD) exceeds a threshold, keeping on using the Li-Po battery not only leads to its quickly depletion but also compromises the battery lifetime. Next, we detail the use of a drone energy consumption model in order to apply this conservative approach for deciding on n wherein this threshold is fixed to 80%.

Notice that in Eq. (9) we are not considering neither take-off nor landing times, since the energy consumption involved in both maneuvers has a negligible as compares to that of the long runs of horizontal flight. We follow D'Andrea (2014) to calculate the energy per meter in steady level flight considering that the fundamentals forces are thrust to move forward, weight from gravity action on the UAV mass, and lift and drag. Thus, on assuming a flight at a constant altitude and constant speed, the energy per meter can be expressed in terms of the lift-to-drag (a constant for steady flight), LtD, the UAV mass (summing up the frame mass m^{frame} and the payload mass $m^{payload}$), the percentage of battery energy that we are effectively transferring to motors and propellers, Ω, and the flight speed. There are two modalities of steady level flight in our surveillance application: one at flight speed V^{cruise} and other at flight speed V^{patrol}. The power consumption at each one can be obtained by multiplying the energy per meter by the corresponding constant velocity, and adding the power consumption of avionics (POW^{Avio}):

$$POW^{cruise} = 3.6 \frac{(m^{frame} + m^{payload})}{370\Omega \cdot LtD} V^{cruise} + POW^{Avio} \quad (11)$$

$$POW^{patrol} = 3.6\frac{m^{frame} + m^{payload}}{370\Omega \cdot LtD}V^{patrol} + POW^{Avio} \quad (12)$$

Observe that 3.6 is the conversion factor applied to our velocity in m/s to convert it into km/h as considered in D'Andrea (2014). We recall here that the units in use are: kg for masses (m^{frame}, $m^{payload}$), m/s for velocities (V^{cruise}, V^{patrol}) and kw for the powers (POW^{cruise}, POW^{Avio},POW^{patrol}).

As for the total battery energy, we start from the usual data on capacity and voltage that the manufacturer provides to established it as: Battery_in_KJ= Cap (in Ah) * Voltage (in V) * 3.6. In order to avoid the work of batteries within their accelerated depletion range, the number of Joules to plan on every flight are limited to a battery energy bound, BEB:

$$BEB = 80\% \cdot 3.6 \cdot Cap \cdot Voltage \quad (13)$$

This energy BEB should be enough to cover the cumulative energy consumed along the three steady flight sections (namely, at constant altitude along with velocity V^{patrol} when patrolling the perimeter and V^{cruise} while approaching or leaving the perimeter) within each flight mission. Then,

$$1000 \cdot \left[\frac{L \cdot POW^{cruise}}{V_{cruise}} + n \cdot T^r \cdot POW^{patrol} + \frac{(R-r) \cdot POW^{cruise}}{V_{cruise}}\right] \leq BEB \quad (14)$$

3.1.4 Fleet Size on assuming a constant number of UAVs per base station

As we will explain, the whole number of drones w can be expressed as a function of the distance from the take-off point to the perimeter (L), the time elapsed for patrolling every sector (T^r), the number of sectors which the UAV guard on every single flight (n), the recharging time ChT at the ground charging stations and the number of sectors S. We explain the reasoning based on the example depicted in Fig. 4 as follows.

Let us inspect what occurs in-between a drone arrives at the perimeter at point P_{i+1}, and it is back to revisit this point again: it patrols n segments (out of the S in which we split the perimeter) in a $n \cdot T^r$ time, then flies a radial distance $R - r$ to reach a ground

recharging point, then stay charging during ChT seconds and later takes-off and travels along L meters to reach again the perimeter (at point P_{i+n+2}). Hence, the number of UAVs that would be necessary for persistently guarding each one of this n sectors can be computed like this: The whole time lagged since one particular UAV take-off two consecutive times is $n \cdot T^r + \frac{(R-r)}{V^{cruise}} + ChT + \frac{L}{V^{cruise}}$, and consequently, if we divide this into the revisiting time established for any sector, T^r, we obtain how many drones are needed to guard the n sections involved in our discussion –see Fig. 4- with the requested periodicity, T^r. However, our purpose is to define the size of the fleet capable of persistently guarding the whole circle perimeter, from which we have to multiply by a factor $\frac{S}{n}$ and round up in order to find the fleet size:

$$w = \left\lceil \frac{S}{n} \cdot \frac{\frac{L}{V^{cruise}} + \frac{(R-r)}{V^{cruise}} + n \cdot T^r + ChT}{T^r} \right\rceil \tag{15}$$

Finally, we will assume there is a preference on having exactly the same number of drones assigned to each base station. This leads us to a slightly different fleet size w^s as the one to be ultimately used in our system:

$$w^s = S \cdot \left\lceil 1 + \frac{\frac{L}{V^{cruise}} + \frac{(R-r)}{V^{cruise}} + ChT}{nT^r} \right\rceil \tag{16}$$

Therein it is clear that the suggested fleet size w^s is above the number of bases S. For instance, the example shown in Fig. 4 has considered that $ChT = 5600\text{s}$ and $E = 3000\text{s}$, from which Eq. (9) along with Eq. (8) lead to a fleet of $w^s = 36$ (different to the minimal fleet required which was $w = 32$). Thus, our symmetric pattern for this persistent surveillance consists of splitting the circular area into $S = 9$ sectors, served with 9 base stations wherein we settle 4 UAVs to be able to continuously monitoring the perimeter at a period of $T^r = 1182s$, each UAV's flight covering $n = 2$ sectors.

3.2. Compact formulation extended to a variety of drone platforms

In order to decide among a variety of commercial drone platforms $p \in P$, a binary selection variable α_p is introduced for selecting the more appropriate one, along with the

mobility pattern for the defined swarm patrolling circular perimeter. Hence, the decision variables described in the above reasoning are transformed to account for the concerned drone platform p (namely, w_p^s,r_p, T_p^r,L_p,S_p,V_p^{cruise}, POW_p^{cruise}, POW_p^{patrol}). The comprehensive non-linear MILP model to cope with such decisions – see Table 1 for notations- is as follows:

Table 1. MATHEMATICAL MODEL NOTATIONS

Sets	
P	The set of commercial drone platforms under consideration.
Parameters	
R	The radius of the circular perimeter, expressed in meters.
MRT	Maximal span time between revisits every point in the perimeter, measured in seconds.
V^{patrol}	The patrolling velocity, fixed at 2 m/s.
r_{max}	The upper bound to the radius for placement of the base stations.
d_{max}	The maximal range for communications for a flight mission.
POW^{Avio}	Power consumption due to the camera on-board, no matter which platform $p \in P$, measured in kwatts.
E_p	Maximal flight time or Endurance for the platform $p \in P$.
m_p^{frame}	The mass of the frame of the commercial platform $p \in P$, measured in kg.
$m^{payload}$	The mass of the payload (other than the common camera) installed on the commercial platform $p \in P$, measured in kg.
Ω_p	Efficiency in the transference of electrical energy to motors and propeller, according to the specifications of platform $p \in P$. It stands for the percentage of the power drawn at batteries that is effectively converted in power used by the propeller.
LtD_p	The lift-to-drag ratio which combines in a single parameter the aerodynamic and drone design aspect for each commercial platform $p \in P$.
BEB_p	The limit to the battery energy drained on every flight mission, dependent on the features of the platform $p \in P$. The bounded number of KJoules to consider are limited to a value $BEB_p = 80\% \cdot 3.6 \cdot Cap_p \cdot Voltage_p$, where Cap_p is the capacity in Ah and $Voltage_p$ is the voltage according to the specifications for the Li-Po batteries set on board of the commercial platform $p \in P$.
Variables	
α_p	Binary variable. Takes value 1 if the platform $p \in P$ is selected.
S_p	Integer number of segments in which we are dividing the circular perimeter, in the event that the platform $p \in P$ is selected.
w_p^s	Integer number of drones in the fleet for a symmetric pattern for the persistent surveillance –i.e, with equal number of drones at every base station- , in the event that the platform $p \in P$ is selected.
n_p	Integer number of segments that a platform $p \in P$ patrols, in the event that the platform $p \in P$ is selected. For each platform p, n_p varies within the interval [1,S_p].
δ_p	The angle of each sector in which we are splitting the circle, in the event that the platform $p \in P$ is selected.
r_p	The radius of the inner circle where we place the S_p equally distributed base stations.

L_p	The distance from the source base station to the points where the control of the flight mission of platform $p \in P$ is transferred to the next base station, in the event that the platform $p \in P$ is selected.
T_p^r	The revisit time, namely, the time elapsed for patrolling every sector on platforms of type $p \in P$, in the event that the platform $p \in P$ is selected.
V_p^{cruise}	The velocity that platform $p \in P$ uses on moving to or returning from the perimeter, in the event that the platform $p \in P$ is selected.
POW_p^{cruise}	The power consumption considered from steady level flight at velocity V_p^{cruise}, in the event that the platform $p \in P$ is selected.

$$Min \sum_{p \in P} \alpha_p \cdot T_p^r \cdot w_p^S \quad (17)$$

$Subject\ to$:

$$r_p \leq r_{max} \qquad p \in P \ (18)$$

$$L_p^2 = 4R\, r_p \cdot \sin^2\left(\frac{\delta_p}{2}\right) + (R - r_p)^2 \qquad p \in P \ (19)$$

$$L_p \leq d_{max} \qquad p \in P \ (20)$$

$$T_p^r \leq MRT \qquad p \in P \ (21)$$

$$S_p \cdot \delta_p = 2\pi \qquad p \in P \ (22)$$

$$T_p^r = \delta_p \cdot \frac{R}{V^{patrol}} \qquad p \in P \ (23)$$

$$\frac{L_p}{V_p^{cruise}} + n_p \cdot T_p^r + \frac{R - r_p}{V_p^{cruise}} \leq E_p \qquad p \in P \ (24)$$

$$POW_p^{cruise} = 3.6 \cdot \frac{m_p^{frame} + m^{payload}}{370 \cdot \Omega_p \cdot LtD_p} \cdot V_p^{cruise} + POW^{Avio} \qquad p \in P \ (25)$$

$$POW_p^{patrol} = 3.6 \cdot \frac{m_p^{frame} + m^{payload}}{370 \cdot \Omega_p \cdot LtD_p} \cdot V^{patrol} + POW^{Avio} \qquad p \in P \ (26)$$

$$1000 \cdot \left[\frac{L_p \cdot POW_p^{patrol}}{V_p^{cruise}} + n_p \cdot T_p^r \cdot POW_p^{patrol} + \frac{(R - r_p) \cdot POW_p^{patrol}}{V_p^{cruise}}\right] p \in P \ (27)$$

$$w_p^s = S_p \cdot \left\lceil 1 + \frac{\frac{L_p}{V_p^{cruise}} + \frac{R - r_p}{V_p^{cruise}} + ChT}{n_p \cdot T_p^r} \right\rceil \qquad p \in P \ (28)$$

$$\sum_{p \in P} \alpha_p = 1 \qquad (29)$$

$$SpeedMin_p \leq V_p^{cruise} \leq SpeedMax_p \qquad p \in P \ (30)$$

$$r_p\,, T_p^r, L_p, S_p, V_p^{cruise}, POW_p^{cruise}, POW_p^{patrol} \geq 0 \qquad p \in P \ (31)$$

$$\alpha_p \in \{0,1\}, \ \ n_p, w_p^s \ integer \geq 0 \qquad p \in P \ (32)$$

It is worth commenting that by appointing the above non-linear MILP model at the minimization of the product $T_p^r \cdot w_p^s$ for the selected platform, we are indeed obtaining a trade-off between the pursued fleet size minimization and the span of the revisits to the perimeter.

Note that, from a resolution point of view, the above formulation allows us for decomposing the problem into a set of sub problems, each one corresponding to a specific platform, i.e., the model could be solved, one by one, for each one of the drone platforms. However, since the number of variables and constraints of the complete formulation is small, it is not necessary to carry out this decomposition. It should be noted that along with the best design (that from the selected platform), the compact model resolution also determines a feasible design for each of the considered platforms.

We refer the reader to Fig. 5 for an example giving a complete picture on how a persistent surveillance can be set up around a swarm of drones, everyone with a cyclic schedule of flight missions with non-coincident take-off and landing base stations.

Since we need to ensure the robustness of the operational design of our persistent surveillance system, every cyclic patrol scheduling of the circular perimeter that could arise from solving the above optimization model (17)-(32) (namely, the chosen drone platform to use to revisit each of the sectors in which we split the perimeter every T_p^r, the

allocation of a number of drones at each base station, which are located at r_p meters from the centre) need to be further studied to assess the expected robustness performance.

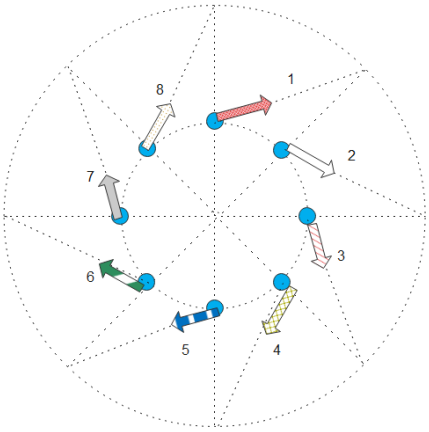

(a) Start of the surveillance. Drones take off from base stations ($t = 0$).

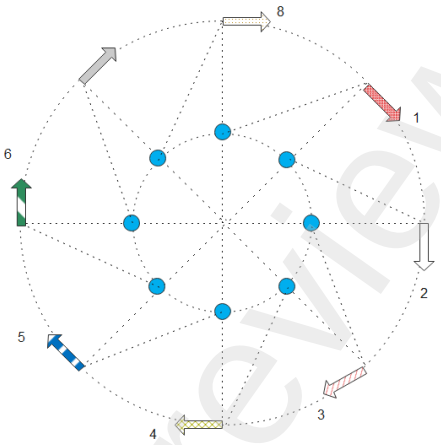

(b) The drones reach the perimeter and start patrolling the first sector ($t = L/V_{cruise}$).

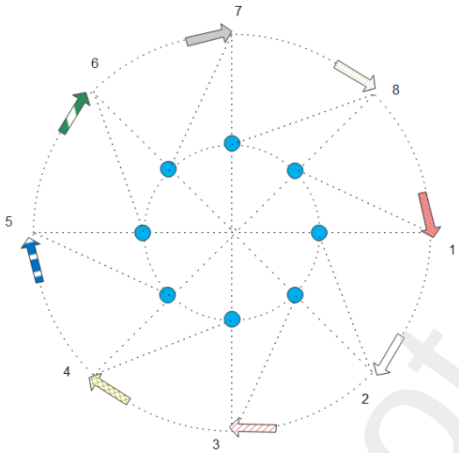

(c) The drones reach the end of the first sector. A new set of drones are prepared at the base stations ($t = L/v_{cruise} + T^r$).

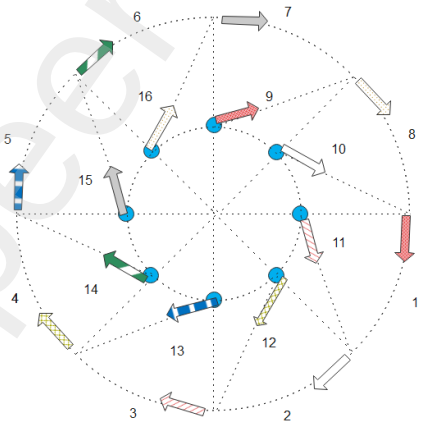

(d) The new set of drones take off from the base stations when the first set of drones start patrolling their second sector ($t = \frac{L}{v_{cruise}} + T^r + \Delta$).

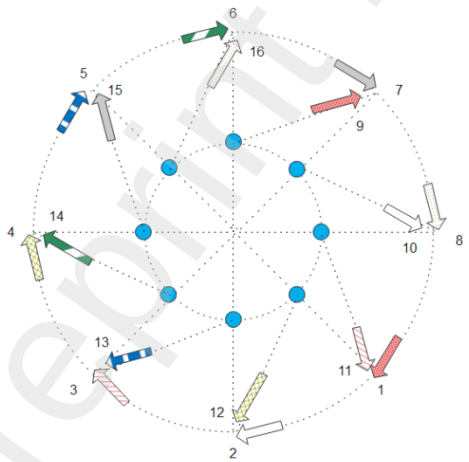

(e) When the first set of drones are finisihing the patrolling of their second sector, the new set of drones are coming to the permeter ($t = L/v_{cruise} + 2T^r$).

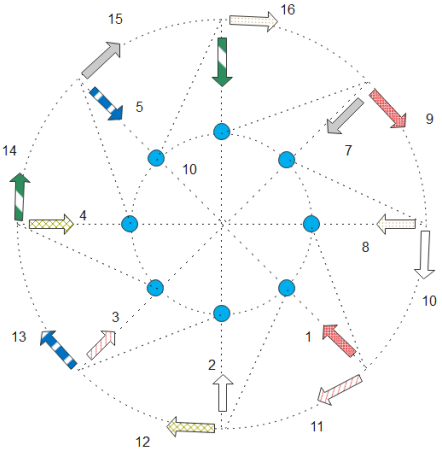

(f) The first set of drones come back to the base stations to be replenished. The second set of drones start the patrolling of their first sector ($t = \frac{L}{v_{cruise}} + 2T^r + \Delta$).

Fig. 5. Example of the persistent patrolling service on a swarm of 16 drones flying at the same time, each of which serves 2 segments when the perimeter is divided into 8 sectors: (a) Take-off from source base stations, (b) Init of the first patrol, (c) End of the first patrol, (d) Take-off of the second drone at each base station, (e) End of second patrol, and (f) Return of the first set of drones at a different base station.

4. Robustness of the Cyclic Surveillance Service

In this section, we present a DES model to check the extent to which a cyclic patrol design exhibits an appropriate protection against the accelerated depletion of batteries as an uncertainty source limiting the flight of UAVs.

On solely considering the specifications from cells manufacturers, many reported UAV's applications have in fact neglected the dynamic behaviour of their energy storage. Recently, Chen et al. (2019) have contributed with a novel battery-aware model that allows for estimating better the point of accelerated depletion of batteries. While Chen et al. (2019) claim that the energy consumption is a function of weight, distance and flight speed, we are in a case study wherein the latter is the only control variable; our surveillance drone has always the same mass, and the distances to cover in the involved ISR missions are fixed. Hence, on studying the uncertain flight times (endurance) we consider the electrical power required as a function of the cruise velocity (Dukkanci et al. 2021; Zeng et al., 2019; Zhang et al., 2021). We have applied a similar shape to that in Zeng et al. (2019) for the propulsion power consumption for rotary-wing UAVs (steady level flight at $V^{cruise} or\ V^{patrol}$ speed) –see Fig. 6-, since in all the cases the drones to be selected in our practical scenario are multi-rotor UAVs. Nevertheless, we recall here that we do not attempt to use the shape to select the flight velocity but solely to calculate the per-meter flight energy consumption.

One of the settings within our DES model is the likelihood of failure –namely, aborting beforetime the mission of a UAV because of being too close to the battery discharging time- as a function of DOD. Importantly, we are concerned with long distances travelled and neglect both the take-off and landing consumptions, so we firstly evaluate DOD from the power consumption cumulated on the flight mission computed by entering in Fig. 6 with $V^{cruise} or\ V^{patrol}$, then multiplying by the respective known distances and then summing up. We secondly used the obtained DOD as an input to a new shape used to sample the likelihood of running out of battery in a certain simulation of the DES model. Particularly, we propose a piecewise linear function –see Fig. 7 - wherein a risk of failure in the flight mission (as a probability value) appears beyond a threshold point at a DOD^{th}

=80% of the nominal energy of the Li-Po battery whose depletion is let to be up to 5% deeper (namely, up to 82,4% which leads to a risk of failure of 12%).

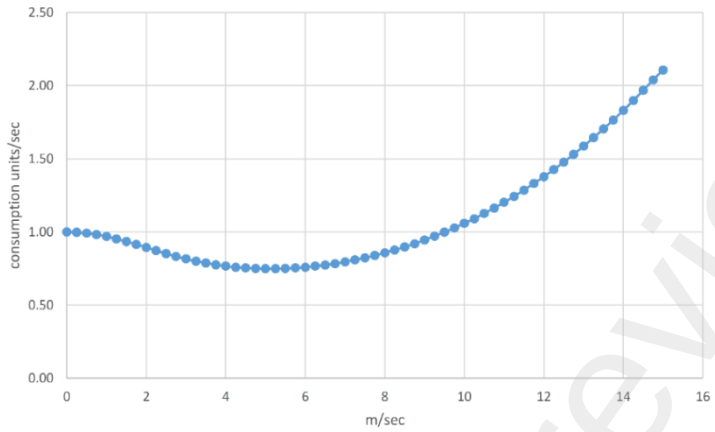

Fig. 6. The power consumption as a function of the UAV speed

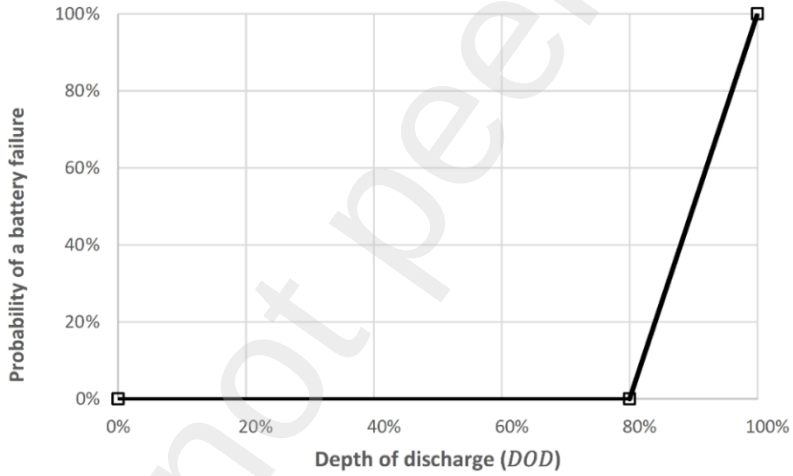

Fig. 7. Probability of a battery failure as a function of the depth of discharge (DOD).

The standard flight mission for every UAV within our simulated persistent surveillance system of the circular perimeter is modelled according to the flowchart in Fig. 8. There are three steps within every drone mission: *(i)* Take-off and transfer from the base station to the perimeter, *(ii)* Surveillance of a number of assigned sectors and *(iii)* Return to another base station. As is shown in step *(iii)*, once a UAV returns to a base station a battery replenishment process take place. After the recharging time (ChT), this UAV becomes active again.

In our DES model we check in advance the DOD that we would have at the end of the next sector before starting to patrol that sector. If it would be at a $DOD > DOD^{th}$ a failure signal is sent to the system, since a risk of running out of battery is identified. This way we model the risk of failing at a certain point while in *(ii)*. Once the failure is present, the involved UAV is marked to be substituted for patrolling the next sector as planned and commanded to return to a different base station than the initially planned. In parallel, a relay UAV is then invited to take-off with sufficient time to start surveying the non-covered sector on time.

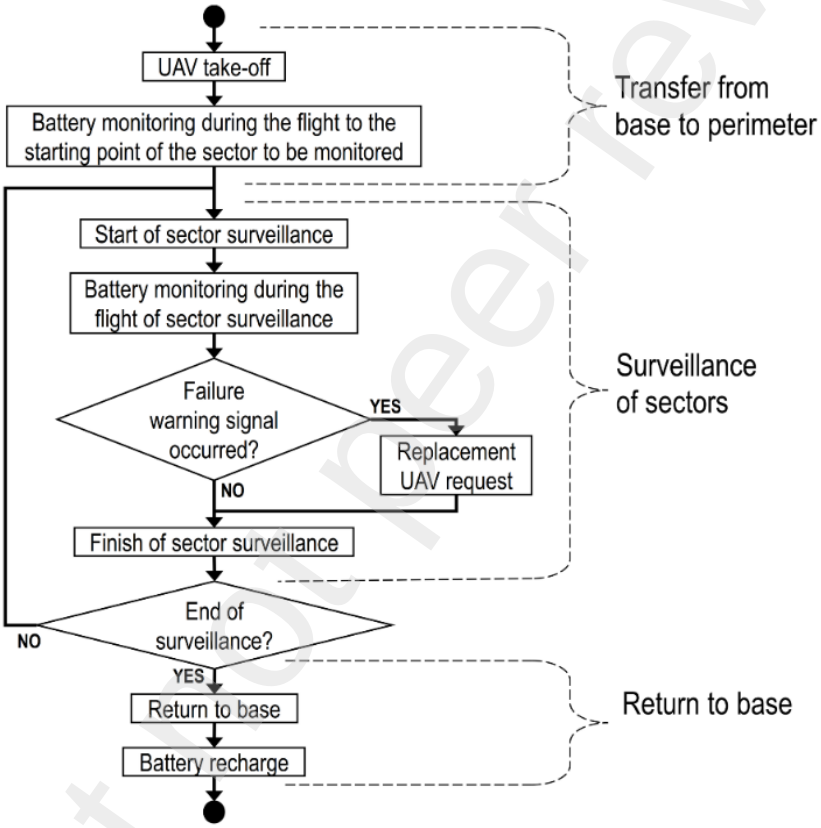

Fig. 8. Operation diagram of a surveillance flight mission.

In Fig. 9 we present an example that illustrates how the system could recover from a single battery failure, ultimately providing an on-time service. Observe how, starting from a balanced distribution of idle drones among the base stations (which is logical in a symmetrical system like ours), this symmetry is broken once the relay procedure occurs.

The priority among the bases from which picking up the substitute drone is as follows. Firstly, a request for an idle drone is directed to the base wherein the failing drone will

land –i.e., a sort of swap between the failing and the idle drone-, since in case there is a ready drone there this provides the quicker response to the disruptive event. If not, an

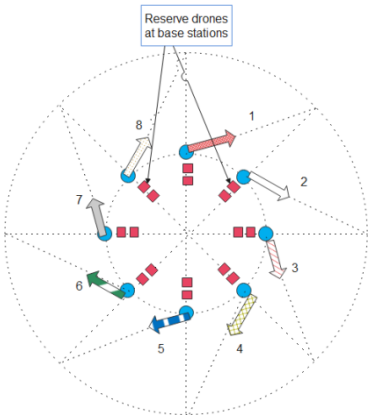

(a) Start of the surveillance. Drones are launched from base stations ($t = 0$).

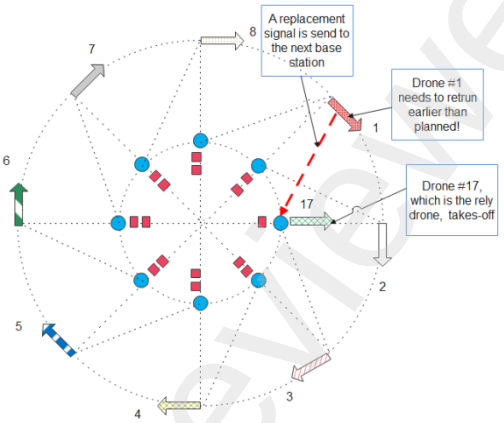

(b) First lot of drones are patrolling their 1st sector. While doing it, Drone#1 discovers its battery is draining and needs to returns as soon as the current sector patrolling is finished. Let's suppose that Drone#17 is the relay drone ($t = L/v_{cruise} + 0.1\ T^r$).

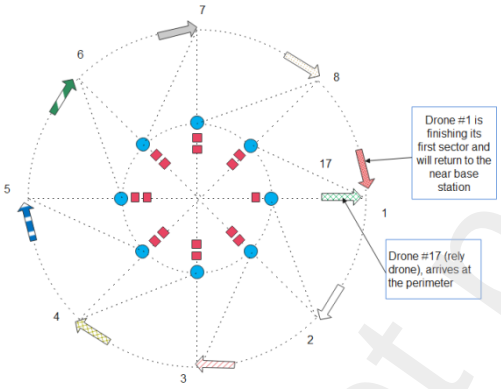

(c) The substitute drone takes off so as to be on-time to relay the failing drone: the involved sector will be punctually covered ($t = L/v_{cruise} + 0.9\ T^r$).

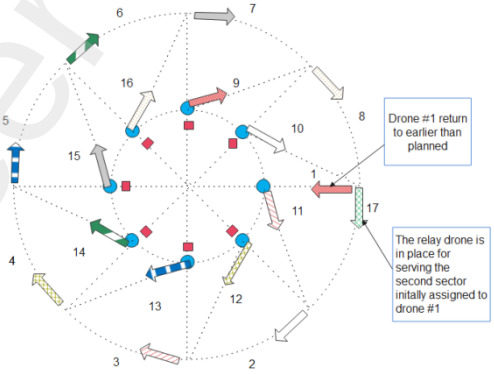

(d) At the same time that the first lot finalize the 1st sector, the second lot of drones are launched according to plan. The relay Drone#17 is in place for serving the sector that the failing Drone#1 could not, and the Drone#1 returns to the appropriate base station ($t = L/v_{cruise} + T^r + \Delta$).

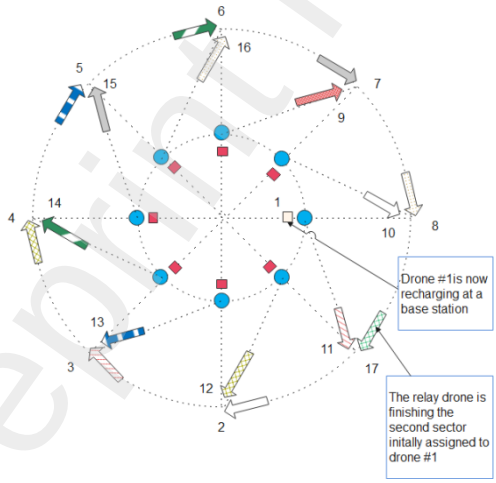

(e) The first set of drones are finishing the patrolling of their 2nd sector, and the relay drone is finishing its service as well (the substitute drone only serves the remaining sector/s uncovered by the failing one). The new set of drones are almost reaching the perimeter ($t = L/v_{cruise} + 2T^r - \Delta$).

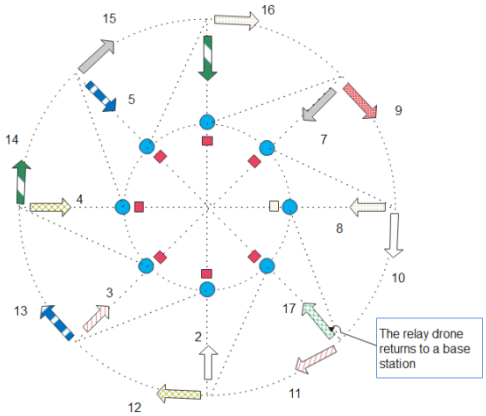

(f) The first set of drones come back to the base stations. The second set of drones start the patrolling of their 1st sector ($t = \frac{L}{v_{cruise}} + 2T^r + \Delta$). The relay drone leaves the perimeter and moves to the nearer base station.

Fig. 9. Example of the relay procedure on a system with 8 sectors and 2 segments per flight: (a) Take-off from source base stations, (b) Init of the first segment patrol, (c) Take-off of the second lot of drones at each base station and init of second patrol, except for the relay which will serve only its first segment, (d) End of second segment patrol, and (f) Return of the first set at a different base station.

attempt will be made to choice the relay drone from the previous base station, in case there is a ready drone on it (the substitute drone reachs the involved sector throughout an oblique flight). If this is not possible either, an attempt will be made to launch the relay drone from the rear base station –an oblique flight, this time backwards-, in case there is a ready drone on it. Finally, if the latter is not yet possible, the only option is to stay waiting for a drone to be available at the base wherein the failing drone will land.

Please notice that it is possible that the described relay mechanism could lead to ultimately monitoring the involved sector with a certain delay (we mark it as delayed when the lag time is $>0.05\ T^r$). Even more, providing that the hypothetical starting time for the relay drone exceeds T^r, the emergency surveillance of the involved sector is indeed cancelled. In that case, since the next drone in the cyclic patrolling schedule arrival is expected in a time T^r, the relay itself has non-sense.

Noticeably, the drone fleet is shared over time by all the base stations. We defined a cyclic schedule of the flight missions but with non-coincident start (take-off) and end (landing) points for every drone and further, every battery failure produces a dynamic imbalance between the drones available in the different bases derived from the relay procedure that it triggers. The number of sectors patrolled with delay and the number of cancelled/ unattended sectors are the output indicators measured from the long runs of execution of the designed DES model, to ultimately assess the robustness of the persistent surveillance service provide by a certain fleet size.

5. Computational Experiments

In this section, we first test the proposed non-linear MINLP formulation using the solver of DICOPT (Grossmann et al., 2002). Specifically, we have considered the alternative drone platforms showed in Table 2 when seeking for the cyclic patrolling schedule for the list of target areas in Table 3. Our computational experience – an x64bits computer with Intel Core i7-4712MQ 2.8Ghz processor and 16 GB of RAM- showed that the non-linear DICOPT solver within GAMS is able to provide us optimal solutions in

less than 600s in all the cases. Importantly, on obtaining the solutions reported in Table 3, we considered solely the drone platform features included in the MILP stated in Section 3, without any reference to its purchasing costs, manoeuvrability or reliability.

Table 2. DRONE PLATFORMS CONSIDERED.

	INPUT DATA CONCERNINING THE ALTERNATIVE DRONE PLATFORMS							
	HIGH LEVEL SPECIFICATIONS			*AERODYNAMICAL &ELECTRICAL SETTINGS*			*SURVEILANCE FLIGH SPEED*	*AVIONICS POWER CONSUMPTION*
UAV LABEL	$m_p^{frame} + m^{paylo}$	*SPEED*	E_p	Ω_p	LtD_p	Cap_p & $Voltage_p$	V^{patrol}	POW^{Avio}
MARVIN-5	[6.40 + 0.35] kg	[9,36]	1600	0. 5	1.8	21 & 22.8	2	0.1 Kw
DJI-M210	[6.00 + 0.35] kg	[8,36]	3000	0.65	1.5	15.33 & 22.8	2	0.1 Kw
TAROT-500	[2.15 + 0.35] kg	[9,45]	1580	0.65	1.6	5.3 & 22.2	2	0.1 Kw
MD4-1000	[3.80 + 0.35] kg	[10,44]	3450	0.65	1.6	5.3 & 22.2	2	0.1 Kw

Table 3. THE MILP WITH DIFFERENT INPUTS PARAMETERS PROVIDES DIFFERENT DESIGNS.

		Design1	***Design2***	***Design3***	***Design4***	***Design5***	***Design6***
Input Parameters	*Radius*	R=1196 m	R=1496 m	R=1696 m	R=1696 m	R=1696 m	R=1696 m
	Maximal comms link	d_{max}=1444 m	d_{max}=1444 m	d_{max}=1444 m	d_{max}=1444 m	d_{max}=1444 m	d_{max}=900 m
	Far Placement of Base Stations	r_{max}=900 m	r_{max}=1333 m	r_{max}=1333 m	r_{max}=1333 m	r_{max}=900 m	r_{max}=1333 m
	Patrolling velocity	$V^{patrol} =$ 2 m/s	$V^{patrol} =$ 2 m/s	$V^{patrol} =$ 2 m/s	$V^{patrol} =$ 2 m/s	$V^{patrol} =$ 2 m/s	$V^{patrol} =$ 2 m/s
	Patrolling recurrence	$MRT =$ 1222 m	$MRT =$ 1222 m	$MRT =$ 1222 m	$MRT =$ 1222 m	$MRT =$ 1222 m	$MRT =$ 1222 m

	Recharging time	ChT =4000 s	ChT =3600 s	ChT =4000 s	ChT =5600 s	ChT =5600 s	ChT =3600 s
Operational Design of the Cycle Patrol Schedule	*Selected Drone* (p*)	MD4-100 MICRODONES	MARVIN-5	MD4-100 MICRODONES	M210-DJI	MD4-100 MICRODONES	MD4-100 MICRODONES
	Radial distance to the center	r =809.15 m	r =1333 m	r =1333 m	r =1333 m	r =900 m	r =1333 m
	Number of sectors	S=4	S=7	S=7	S=8	S=10	S=12
	Number of sectors to monitor in every flight	n=3sectors	n=2sectors	n=4 sectors	n=4 sectors	n=6 sectors	n=7sectors
	Number of UAV per base station	$w^s = 12$ [#3 per Base Station]	$w^s = 28$ [#4 per Base Station]	$w^s = 21$ [#3 per Base Station]	$w^s = 32$ [#4 per Base Station]	$w^s = 30$ [#3 per Base Station]	$w^s = 36$ [#3 per Base Station]
	Transfer speed (to perimeter or back from the perimeter)	$V^{cruise} = 12.22$ m/s	$V^{cruise} = 10$m/s	$V^{cruise} = 12.22$ m/s	$V^{cruise} = 10$m/s	$V^{cruise} = 12.22$ m/s	$V^{cruise} = 12.22$ m/s
	Margin on comms	$L = 1444$ m	$L = 1236.21$ m	$L = 1354.32$ m	$L = 1206.69$ m	$L = 1103.02$ m	$L = 858.80$ m
	Flight Time. = E_{p*} - [Slack of Eq.20]	2967.81 s	1482.78 s	3185.16 s	2821.04 s	3352.26 s	3208.05 s
	Span between revisits	$T^r = 939.34$ s	$T^r = 671.40$ s	$T^r = 761$ s	$T^r = 666$ s	$T^r = 532.81$ s	$T^r = 444$ s

Since system robustness is a fundamental operational feature, we have developed a DES model of the persistent system as a Python application based on SimPy module. Next, we report how this application has been utilised to investigate to what extent any of the cyclic patrol scheduling under consideration is robust enough to the uncertain battery discharging times. Otherwise, it should not be validated as our operational design choice for the targeted persistent surveillance system.

We have conducted two independent robustness studies: (a) Study of the fleet size influence on the robustness of the performance and (b) Study of the influence of design decisions under a similar fleet size.

4.1 Study (a): Effect of the Fleet Size on the Performance of a Cyclic Patrol Scheduling

The study on how the increase of the fleet size can modify the performance of the Surveillance Service is conducted around the preliminary cyclic patrol scheduling presented in Table 4 –namely, the Design3 on Table 3. One hundred of replicas of every scenario are considered, the simulation of each one extending along a horizon of one hundred of complete cycles of surveillance–i.e. the elapsed time at each cycle is $\frac{2\pi \cdot R}{V^{patrol}}$, and a warm-up time is considered before registering the out coming performance indicators. The simulations have been carried out around scenarios generated according to a full factorial design of experiments followed by an ANOVA analysis to the ensure the validity of our insights.

Table 4. THE PRELIMINARY SURVEILLANCE SYSTEM DESIGN & SIMULATION AROUND THE DES MODEL.

1. Input Parameters	*Parameters of the persistent surveillance service*	*Radius of the perimeter circumference*	R=1696 m
		Maximal comms link	d_{max}=1444 m
		Far Placement of Base Stations	r_{max}=1333 m
		Patrolling velocity	$V^{patrol} =$ 2 m/s
		Patrolling recurrence	$MRT =$ 1222 m
	Li-Po Battery parameters	*Recharging time*	ChT =4000 s
2. Operational Design of the	*Selected Commercial Dron*		p*=MD4-100 MICRODONES
	Placement of Base Stations	*Radial distance to the center*	r =1333 m

	Cycle Patrol Scheduling	*Quantity of Base Stations*	*Number of sectors*	S=7
		Number of Sectors patrolled by each single UAV flight mission	*Number of sectors to monitor in a standard flight*	n=4 sectors
		Initial Fleet Size	*Number of UAV per base station*	$w^s = 21$ [#3 UAVs per Base Station]
		Flight Time vs Endurance	$E_{p*} =$ 3450 s	*Flight Time.* = E_{p*} - *[Slack of Eq.20]* = 3185.16 s
		Maximal vs Decided Recurrence	$MRT =$ 1222 m	$T^r =$ 761 s
			Transfer speed (to perimeter or back from the perimeter)	$V^{cruise} =$ 12.22 m/s
3.	***DES setting***			
	Operational characteristics of a standard flight	*Perimetral velocity (over surveillanced sectors)*		2 m/s
		Transfer speed (to perimeter or returning from the perimeter)		110/9 m/s
		Minimum threshold before considering a delayed patrol of sector		5% of the flight time over a sector
	Simulation parameters	*Warm-up period*		50000 s
		Simulated time period in a replica		Time elapsed to complete 100 laps around the perimeter
		Number of replicas		100 replicas

The design of experiments contains two factors as presented in Table 5. The first factor includes four different risk levels (RL) affecting every standard flight. Specifically, RL is set according to the likelihood of interrupting a standard flight, with four different likelihood values: 2.5%, 5%, 10% and 12%. For instance, as the lifecycle of the Li-Po batteries goes on, it is expected that an increasing likelihood will affect the performance of the system. While completing a standard flight involves surveying all assigned sectors and landing at the assigned base, the consequences of a battery failure can be three-fold: *(i)* An on-time service from a relay drone, which forces a readjustment of the cyclic schedules ruling the foregoing surveillance of the perimeter, *(ii)* A delayed service, owing to a feasible degree of delay on the service from a relay drone, and *(iii)* Absence of service on the involved sector when no relay drone can reach the involved sector, at least not in a feasible delay. The second factor is the fleet size (FS), which has been varied ranging from #3 drones per base (namely, the dimensioning resulting from the Optimization model) to #6 drones per base.

Table 5. DESIGN OF EXPERIMENTS FOR STUDY (A).

Factors	Factor 1: RL, Risk Level considered on a standard flight	2.5%, 5%, 10% and 12%
	Factor 2: FS, Fleet sizes	Drones-per-base: #3, #4, #5, #6
Performance indicators	Punctually surveilled sectors (%)	
	Delayed Surveilled sectors (%)	
	Unattended sectors (%)	

In Table 6 we show the F-Statistic and the p-Value obtained in the ANOVA analysis on the three performance indicators measured in this study, for each independent factor (FS and RL) and the interaction between these factors. According to the listed results, the three indicators proposed are affected by each of the two independent factors and also by the interaction between them.

Table 6. RESULT FROM THE TWO-WAY ANOVA FOR STUDY (A).

	Punctually (%)		Delayed (%)		Unattended (%)	
Factors	**F**	**p-value**	**F**	**p-value**	**F**	**p-value**
FS	31242.	0.0	30723.026442	0.0	28278.852504	0.0
RL	2972.907099	0.0	2956.954193	0.0	2597.794509	0.0
FS x RL	1473.811071	0.0	1422.225953	0.0	1412.368775	0.0

Next, we present the performance reports on our DES model simulations in terms of: (a) the percentage of punctually patrolled sectors –i.e., according to the mission plan-, (b) the percentage of sectors delayed in their surveillance, although only suffering a small lag, and (c) the percentage of unattended (cancelled) sectors. The mean values along the run of simulations within the first study (a) are plotted in Fig. 10. The insights are as follows.

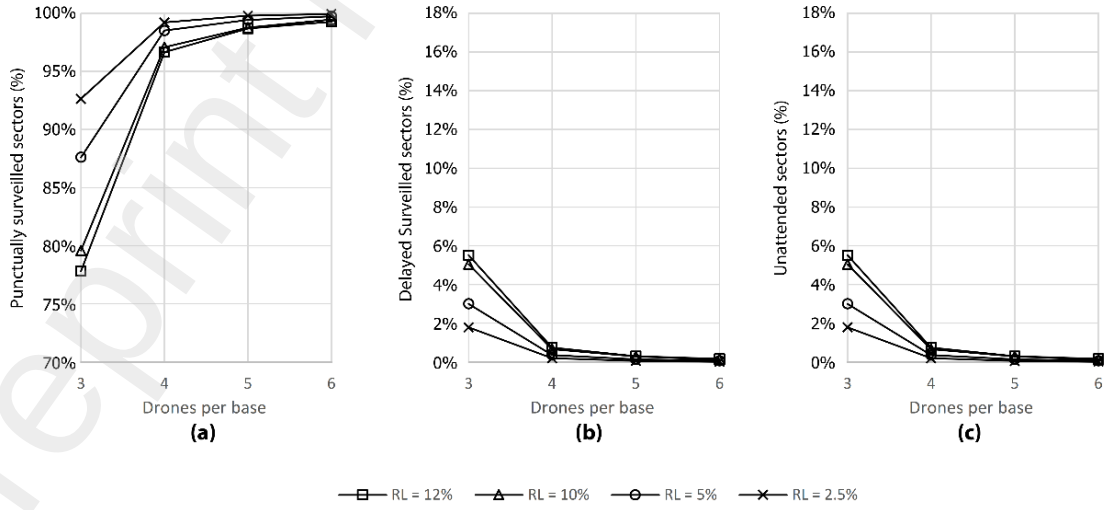

Fig. 10. Testing the effect of FS on the Performance of a Cyclic Patrol Scheduling

Firstly, the probability of battery failure in an individual standard flight under the more optimistic battery assumption RL=2.5% is not null: the global percentage of the punctually patrolled sectors for the original fleet size (#3) reaches only a 92.6%. Hence, there is an unneglectable probability of non-compliance with the planned surveillance task even in the more positive hypothesis on the battery resiliency. This is due to the dynamic imbalance between the drones available in the different base stations that temporarily appear when a battery failure triggers the relay procedures. Obviously, this drawback is stressed in the case of the more pessimistic selection of RL=12%; which results in a 77.8% of unattended sectors. Conversely, as the fleet size increases the robustness of the global mission plan is expected to improve, and more and more punctual surveillance of the sectors are attained. With the solely allocation of an additional drone per base (#4, a 33% increase in the fleet size) the new punctual surveillance scores range from 99.3% at RL=2.5% to 96.7% at RL=12%. While further increasing the fleet size (#5 and #6) improves the robustness regarding the attendance of sectors, we conclude that #4 gives up a satisfactory proportion of above the 96.7% on the punctuality on patrolling each sector.

Secondly, concerning the number of delayed sectors, the surveillance service provides a delay a probability of 16.7% under a RL= 12%, whereas this score is reduced to a 5.6% when RL=2.5%. Again, the addition of drones should lead to cutting the delays down. With the solely allocation of an additional drone per base (#4, a 33% increase in the fleet size) the variation in the percentage of lagged sectors range from 0.6% at RL=2.5% to 2.6% at RL=12%.

Finally, the more stringent effect of the uncertain failures on batteries are the absence of a surveillance service on certain sector. The percentage of unattended sectors for the original fleet size (#3) varies from a 5.51% when RL=12%, to a 1.73% when RL=2.5%. The effect of adding a drone per base station turns into an improvement on this indicator, reaching a 0.19% at RL=2.5% and a 0.73% at RL=12%.

Aside from concluding that the performance can be protected by using more drones in the fleet, we have to highlight also that certain saturation effect appears when the fleet becomes too populated. For instance, the benefit of moving from #5 to #6 is unclear, regardless the fact that a bigger fleet means a greater investment (both, purchasing and maintenance).

4.2 Study (b): Effect of Sectorization on the Persistent Surveillance Performance

Generally, there exist a variety of feasible sectorization patterns that could be the basis to build the required cyclic patrolling schedule. Next, we study the influence that the choice of the sectors partitioning exerts on the robustness of the persistent surveillance service provided by a certain fleet size. Specifically, let us consider that by solving our proposed MILP we obtain the alternative design settings presented in Table 7, wherein the surveillance missions of each flight covers exactly a half of the perimeter in both cases. Simulation studies have been carried out according to a full factorial design of experiments followed by an ANOVA analysis.

Table 7. THE ALTERNATIVE SECTOR PARTITIONING SETTINGS OF EXPERIMENTS FOR STUDY (B).

			Sectorisation SP$6	Sectorisation SP$8
1. MILP Design outcome	*Selected Commercial Dron*		p*=MD4-100 MICRODONES	
	Li-Po Battery parameters	*Recharging time*	ChT =4000 s	
		Patrolling velocity	$V^{patrol} =$ 2 m/s	
	Sectorization pattern	*Radius of the perimeter circumference*	1696 meters	
		Number of sectors	S=6	S=8
		Span between revisits	888 s	666 s
		Placement of Base Stations	249 m	389.66 m
		Transfer speed (to perimeter or back from the perimeter)	8.48 m/s	9 m/s
		Number of sectors to monitor in a standard flight	n=3	n=4
2. DES setting	*Perimetral velocity (over surveillanced sectors)*		2 meters/second	
	Transfer speed (to perimeter or returning from the perimeter)		8.48 meters/second	9 meters/second
	Minimum threshold associated with a delayed surveillance		5% of the flight time over a sector	
	WarmUp period		50000 seconds	
	Simulated time period in a replica		Time elapsed to complete 100 laps around the perimeter	
	Number of replicas		100 replicas	

The design of experiments contains three factors as presented in Table 8. The first factor comprises of two different sector partitioning (SP) for surveillance missions that covers exactly a half of the perimeter: SP$6 (design composed by 6 base stations and 6 sectors) with $n = 3$ sectors patrolled per drone flight, and SP$8 (design composed by 8 base stations and 8 sectors) with $n = 4$ sectors patrolled per drone flight. The second factor includes again the four different risk levels affecting every standard flight. Specifically, RL is set according to the likelihood of interrupting a standard flight, with four different likelihood values: 2.5%, 5%, 10% and 12%. Finally, the third factor evaluates two different fleet size scales (FSS). We firstly evaluate a fleet size of FSS=24 drones (namely, #4 drones per base in the SP$6 scenario and #3 drones per base in the SP$8 design), and then move to evaluate greater fleet size scales: #5 drones per base station in the SP$6 and #4 per base station in the SP$8 (namely, FS=30 and FS=32, respectively).

In Table 9 we show the F-Statistic and the p-Value obtained in the ANOVA analysis on the three robustness indicators, for each independent factor (SP, FSS and RL) and for the double and triple interaction between these factors. According to the listed results, the three indicators proposed are affected by each of the three independent factors and also by the interactions between them.

Table 8. DESIGN OF EXPERIMENTS FOR STUDY (B).

Factors	Factor 1: S, Sectorisation	• 3 sectors surveilled per flight from a total of 6 sectors compounding the surveilled perimeter • 4 sectors surveilled per flight from a total of 8 sectors compounding the surveilled perimeter
	Factor 2: RL, Risk Levels considered on a standard flight	• 2.5% • 5% • 10% • 12%
	Factor 3: FSS, Similar Fleet Size Scale	• Size A: 24 drones (#4 Drones-per-base in SP$6, or #3 Drones-per-base in SP$8). • Size B: 30 drones (#5 Drones-per-base in SP$6), 32 drones (#4 Drones-per-base in SP$8),
Performance indicators	Punctually surveilled sectors (%)	
	Delayed Surveilled sectors (%)	
	Unattended sectors (%)	

Table 9. RESULT FROM THE THREE-WAY ANOVA FOR STUDY (B).

	Punctually (%)		Delayed (%)		Unattended (%)	
Factors	**F**	**p-value**	**F**	**p-value**	**F**	**p-value**
S	10035.99	0.00	8452.37	0.00	11513.64	0.00
RL	395.18	0.00	488.91	0.00	294.99	0.00
FSS	8970.40	0.00	8708.39	0.00	8954.63	0.00
S x RL	133.20	0.00	85.46	0.00	190.49	0.00
S x FSS	4644.02	0.00	4076.10	0.00	5126.94	0.00
RL x FSS	103.52	0.00	109.61	0.00	93.99	0.00
S x RL x FSS	93.72	0.00	73.27	0.00	114.95	0.00

Next, we present the performance reports on our DES model simulations in terms of: (a) the percentage of punctually patrolled sectors –i.e., according to the mission plan-, (b) the percentage of sectors delayed in their surveillance, although only suffering a small lag, and (c) the percentage of unattended (cancelled) sectors. In addition, and for the sake of clarity, the performance report on this second run of execution also represents in (d) the proportion of disrupted patrolled sectors (whether delayed or cancelled/unattended) that were finally cancelled sectors. The mean values for these four indicators are plotted in Fig. 11. The insights are as follows.

Obviously, the robustness of the persistent surveillance system decreases when RL increases, as can be seen in (a) for each one of the four simulated scenario that arise from crossing FSS and SP factors. Besides, at a fixed RL, the increase of FSS provides a better performance for both, SP$6 (squares) and SP$8 (triangles).

More interesting insights arise from comparing the different performance from SP$6 and SP$8 under similar value of FSS. A dashed line is used for the results from a value of FSS=24, which clearly show that the SP$6 outperforms the SP$8 for each RL in all the proposed indicators. While the SP$6 provides punctual surveillance in a range 95.1-96.9%, the figure decreases to 76.3-86.9% for the SP$8 case. Similarly, the delayed sectors range 7.1-12% and the cancelled sectors range 7.0-11.9% for the SP$8 are clearly outperformed by that from SP$6 (respectively, the ranges are 1.6-3.1% and 1.5-1.8%). The reason is that the SP$6 solution is considering a reserve drone per base station, whereas the SP$8 is not.

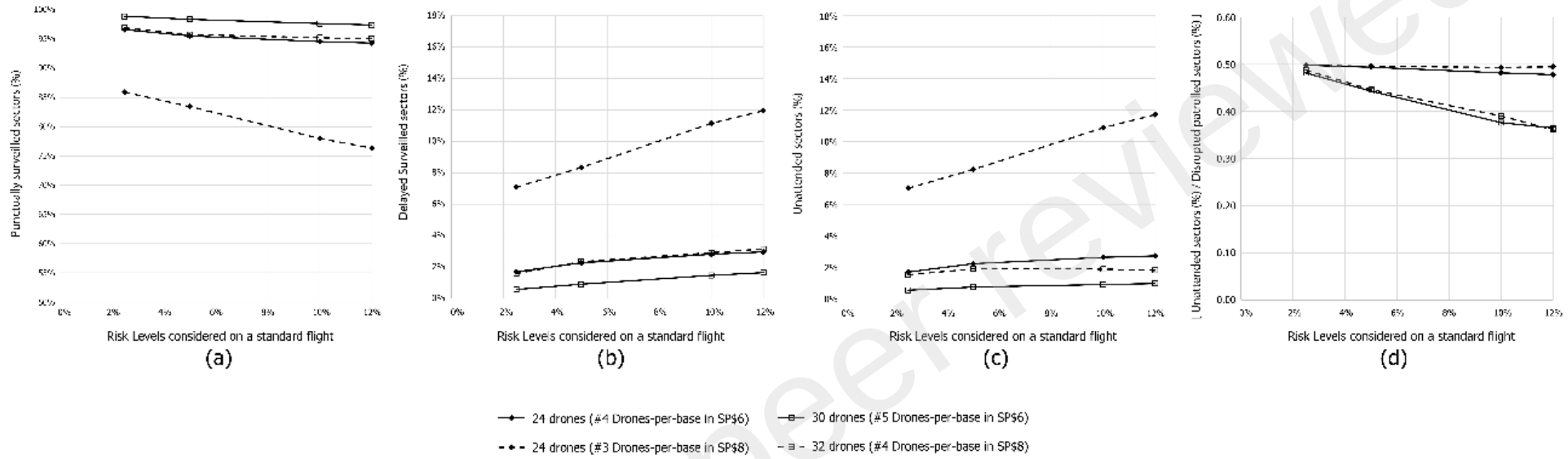

Fig. 11. Testing the effect of Sectorization on the Performance of a Cyclic Patrolling Schedule

In order to analyse the effect of adding a reserve drone also to the SP$8, we refer to the continuous lines used in Fig. 11 to assess how it results as compares with a similar fleet size scale on the SP$6 case. Noticeable, a high robustness is also obtained in the case of SP$8 (punctual surveillance in a range of 94.3-96.1%), indeed quite similar to the SP$6 with #4. In short, the addition of a reserve drone is positive in both partitions, providing a persistent surveillance service wherein the span between revisits is indeed slightly better in the SP$8 (666s). However, the advantage of the SP$6 need to be stressed: it requires a fleet of 24 drones whereas the SP$8 required a fleet of 32 drones for obtaining the same degree of robustness.

6. Conclusions

Despite the recent advances in the UAV technology can potentially lead to more and more completely automated UAV swarm systems, how to allocate tasks to achieve team behaviour is still an open stream of research.

This papers copes with a security-related application wherein a set of camera-equipped UAVs are used for guarding the circular perimeter of a vast restricted area by means of regular patrolling above a minimum patrolling frequency. We have developed a non-linear MILP model aimed at minimizing the ratio between the fleet size and the frequency of revisit, selecting the specific drone platform to use and determining the best cyclic patrol scheduling. We have also developed a DES model for the drone-based persistent patrolling system to check the extent to which a certain fleet size is robust against the uncertain flight time effect. Indeed, any realistic approach to our real-life drone-based system needs to consider the existence of recovery mechanisms to react to uncertain battery failures.

Our proposal consists on placing idle drones at the base stations ready to be incorporated to the system in the event of an early than planned battery depletion. Owing to the symmetrical nature of our circular perimeter surveillance system, it is logical an attempt of balanced distribution of the idle drones among the base stations. Our goal is defining a relay procedure that (with a sufficient likelihood) succeeds in the patrolling of the sector/s that the battery-drained drone could not.

Our assumption is that every battery failure triggers a recovery mechanism whose result can be:

- *(i)* An on-time service from a relay drone, which forces a readjustment of the cyclic schedules ruling the foregoing surveillance of the perimeter,
- *(ii)* A delayed service (lag time is $>0.05\ T^r$), owing to a feasible degree of delay on the service from a relay drone, or
- *(iii)* The absence of service on the involved sector when the lag till the hypothetical starting time for the relay drone exceeds T^r (namely, the arrival of the next drone in the cyclic patrolling schedule is expected in a time T^r and no

advantage arises from using the relay drone for the emergency patrolling of the involved sector).

As described along the paper – see the illustrative example in Fig. 9-, with the relay procedure our system is able to recover from the battery failures but at the cost of breaking the balanced distribution of the idle drones among the different base stations. This effect has been observed in the conducted experimentation on its DES model, wherein at every replicated scenario the asymmetries have been moved from one base station to another as long as the running simulation evolved. According to our experiments, the appearing imbalance leads to unneglectable probability of non-compliance with the planned surveillance task even in the more positive hypothesis on the battery resiliency (with failures probability of hardly a 2,5%).

Importantly, the DES model has served the purpose of studying to what extent we need to use a bigger fleet than that resulting from the MILP resolution to attain an acceptable performance. The insight gained from our computational experience is that the improvements derived from adding idle drones exhibit certain saturation effect when the fleet becomes too populated. In our study a 95% on the punctuality on patrolling each sector has been assumed as a sufficient robustness score.

Hence, we have validated our two-step procedure for the design of a drone-based persistent surveillance system on large circular perimeters. The non-linear MILP resolution for getting a feasible design of a cyclic patrolling schedule and its simulation on the DES model for assessing the robustness performance of the persistent surveillance service under uncertain battery discharging time. Further, as demonstrated in our second computational study, we can use the two-step procedure to evaluate alternative designs considering at once variations on both, the fleet size and the sectors partitioning pattern. In short, the robustness of every sectorization pattern along with every fleet size is assessed with the DES model, thereby allowing the planner for deciding the better operational design for the drone-based persistent patrolling system.

Further research will be pointed at better estimating the energy drainage due to the exact payload in use and at the evolution of the recovery mechanism to incorporate the reaction to the eventual catastrophic loss of a member in the fleet (how to preserve the service under a crashed or malfunctioning UAV). Regarding the former, Sarkar et al. (2020) have

proposed regression and deep learning based methods to predict accurately the flight time for any commercial UAV. Since their empirical study comprises of the different UAV flight events, their model offers us indeed a baseline for the UAV flight time prediction while planning our service. As concerns to the resilience of the service after a catastrophic failure on a drone occurs, we have to further investigate how best addressing the request of backup drone and which policies will be appropriated to decide on the recovery procedures – e.g. the position at which we should carry the substitute drone (to become an idle drone ready to be incorporated into our operations)- for better preserving the performance of our persistent surveillance on the circular perimeter.

Acknowledgements

This research was supported by the Universidad de Sevilla and the Junta deAndalucia, grant number US-1381656, financed with FEDER funds.

References

Angelelli, E., & Speranza, M. G. (2002). The periodic vehicle routing problem with intermediate facilities. *European Journal of Operational Research*, *137*(2), 233–247.

Boggio-Dandry, A., & Soyata, T. (2018). Perpetual Flight for UAV Drone Swarms Using Continuous Energy Replenishment. *2018 9th IEEE Annual Ubiquitous Computing, Electronics and Mobile Communication Conference, UEMCON 2018*, 478–484.

Burdakov, O., Kvarnström, J., & Doherty, P. (2017). Optimal scheduling for replacing perimeter guarding unmanned aerial vehicles. *Annals of Operations Research*, *249*(1–2), 163–174.

Chen, Y., Baek, D., Bocca, A., Macii, A., Macii, E., & Poncino, M. (2019). A case for a battery-aware model of drone energy consumption. *INTELEC, International Telecommunications Energy Conference (Proceedings)*, *2018-Octob*.

Cordeau, J. F., Gendreau, M., & Laporte, G. (1997). A tabu search heuristic for periodic and multi-depot vehicle routing problems. *Networks*, *30*(2), 105–119.

Crevier, B., Cordeau, J. F., & Laporte, G. (2007). The multi-depot vehicle routing problem with inter-depot routes. *European Journal of Operational Research*, *176*(2), 756–773.

D'Andrea, R. (2014). Guest editorial can drones deliver? *IEEE Transactions on Automation Science and Engineering*, *11*(3), 647–648.

Dempsey, M. E. (US A. (2014). *Intelligence, Surveillance, and Reconnaissance Joint Force*.

Dorling, K., Heinrichs, J., Messier, G. G., & Magierowski, S. (2017). Vehicle Routing Problems for Drone Delivery. *IEEE Transactions on Systems, Man, and Cybernetics: Systems*, *47*(1), 70–85.

Drucker, N., Penn, M., & Strichman, O. (2016). Cyclic routing of unmanned aerial vehicles. *Lecture Notes in Computer Science (Including Subseries Lecture Notes in Artificial Intelligence and Lecture Notes in Bioinformatics)*, *9676*, 125–141.

Dukkanci, O., & Kara, B. Y. (n.d.). *Minimizing Energy and Cost in Range-Limited Drone Deliveries with Speed Optimization*. 1–33.

Dukkanci, O., Kara, B. Y., & Bektaş, T. (2021). Minimizing energy and cost in range-limited drone deliveries with speed optimization. *Transportation Research Part C: Emerging Technologies*, *125* :102985.

Fauske, M. F., Mannino, C., & Ventura, P. (2020). Generalized periodic vehicle routing and maritime surveillance. *Transportation Science*, *54*(1), 164–183.

Fetisov, V., & Akhmerov, S. (2019). Charging stations with open contact pads for maintenance of aerial robots. *Proceedings - ICOECS 2019: 2019 International Conference on Electrotechnical Complexes and Systems*, 1–6.

Figliozzi, M. A. (2017). Lifecycle modeling and assessment of unmanned aerial vehicles (Drones) CO2e emissions. *Transportation Research Part D: Transport and Environment*, *57*(October), 251–261.

Gonzalez-R, P. L., Canca, D., Andrade-Pineda, J. L., Calle, M., & Leon-Blanco, J. M. (2020). Truck-drone team logistics: A heuristic approach to multi-drop route planning. *Transportation Research Part C: Emerging Technologies*, *114*, 657–680.

Grossmann, I. E., Viswanathan, J., Vecchietti, A., Raman, R., & Kalvelagen, E. (2002). GAMS/DICOPT: A discrete continuous optimization package. GAMS Corporation Inc, 37, 55.

Hartuv, E., Agmon, N., & Kraus, S. (2018). Scheduling spare drones for persistent task performance under energy constraints: Robotics track. *Proceedings of the International Joint Conference on Autonomous Agents and Multiagent Systems, AAMAS*, *1*, 532–540.

Ho, H. M., & Ouaknine, J. (2015). The cyclic-routing UAV problem is PSPACE-complete. *Lecture Notes in Computer Science (Including Subseries Lecture Notes in Artificial Intelligence and Lecture Notes in Bioinformatics)*, *9034*, 328–342.

Kirschstein, T. (2020). Comparison of energy demands of drone-based and ground-based parcel delivery services. *Transportation Research Part D: Transport and Environment*, *78*(December 2019), 102209.

Li, J., Wang, R., Li, T., Lu, Z., & Pardalos, P. M. (2018). Benefit analysis of shared depot resources for multi-depot vehicle routing problem with fuel consumption. *Transportation Research Part D: Transport and Environment*, *59*(February), 417–432.

Liu, Z., Sengupta, R., & Kurzhanskiy, A. (2017). A power consumption model for multi-rotor small unmanned aircraft systems. *2017 International Conference on Unmanned Aircraft Systems, ICUAS 2017*, 310–315.

Mathew, N., Smith, S. L., & Waslander, S. L. (2015). Planning Paths for Package Delivery in Heterogeneous Multirobot Teams. *IEEE Transactions on Automation Science and Engineering*, *12*(4), 1298–1308.

Mersheeva, V., & Friedrich, G. (2015). Multi-UAV monitoring with priorities and limited energy resources. *Proceedings International Conference on Automated Planning and Scheduling, ICAPS*, *2015-Janua*(Layer 1), 347–355.

Morrison, J. K. & J. R. (2014). On the Concerted Design and Scheduling of Multiple Resources for Persistent UAV Operations. *Journal of Intelligent & Robotic Systems*, *74*, 479–498.

Nebl, C., Kotzur, F. O., Koch, D., & Schweiger, H. G. (2020). Prediction of constant power delivery of lithium-ion cells at high loads. *Journal of Energy Storage*, *30*(November 2019), 101552.

Nguyen, M. T., Nguyen, C. V., Truong, L. H., Le, A. M., Quyen, T. V., Masaracchia, A., & Teague, K. A. (2020). Electromagnetic field based WPT technologies for UAVs: A comprehensive survey. In *Electronics (Switzerland)* (Vol. 9, Issue 3).

Nigam, N. (2014). The multiple unmanned Air Vehicle persistent surveillance problem: A review. *Machines*, *2*(1), 13–72.

Otto, A., Agatz, N., Campbell, J., Golden, B., & Pesch, E. (2018). Optimization approaches for civil applications of unmanned aerial vehicles (UAVs) or aerial drones: A survey. *Networks*, *72(4),* 411–458.

Park, H., & Morrison, J. R. (2019). System design and resource analysis for persistent robotic presence with multiple refueling stations. *2019 International Conference on Unmanned Aircraft Systems, ICUAS 2019*, *144*, 622–629.

Nebl, C., Kotzur, F. O., Koch, D., & Schweiger, H. G. (2020). Prediction of constant power delivery of lithium-ion cells at high loads. Journal of Energy Storage, 30(November 2019), 101552.

Saha, A., Kumar, A., & Sahu, A. K. (2017). FPV drone with GPS used for surveillance in remote areas. *Proceedings - 2017 3rd IEEE International Conference on Research in Computational Intelligence and Communication Networks, ICRCICN 2017*, *2017-Decem*, 62–67.

Sărăcin, C. G., Dragoş, I., & Chirilă, A. I. (2017). Powering aerial surveillance drones. *2017 10th International Symposium on Advanced Topics in Electrical Engineering, ATEE 2017*, 237–240.

Sarkar, S., Totaro, M. W., & Kumar, A. (2020). An Intelligent Framework for Prediction of a UAV's Flight Time. *Proceedings - 16th Annual International Conference on Distributed Computing in Sensor Systems, DCOSS 2020*, 328–332.

Schneider, M., Stenger, A., & Hof, J. (2015). An adaptive VNS algorithm for vehicle routing problems with intermediate stops. *OR Spectrum*, *37*(2), 353–387.

Shi, W., Zhou, H., Li, J., Xu, W., Zhang, N., & Shen, X. (2018). Drone Assisted Vehicular Networks: Architecture, Challenges and Opportunities. *IEEE Network*, *32*(3), 130–137.

Stolaroff, J. K., Samaras, C., O'Neill, E. R., Lubers, A., Mitchell, A. S., & Ceperley, D. (2018). Author Correction: Energy use and life cycle greenhouse gas emissions of drones for commercial package delivery (Nature Communications (2018) DOI: 10.1038/s41467-017-02411-5). *Nature Communications*, *9*(1), 94551.

Troudi, A., Addouche, S.-A., Dellagi, S., & Mhamedi, A. (2018). Sizing of the Drone Delivery Fleet Considering Energy Autonomy. *Sustainability*, *10*(9), 3344.

Zeng, Y., Wu, Q., & Zhang, R. (2019). Accessing from the sky: A tutorial on UAV communications for 5G and beyond. *ArXiv*, *107*(12).

Zeng, Y., Xu, J., & Zhang, R. (2019). Energy minimization for wireless communication with rotary-wing UAV. *IEEE Transactions on Wireless Communications*, *18*(4), 2329–2345.

Zhang, J., Campbell, J. F., Sweeney, D. C., & Hupman, A. C. (2021). Energy consumption models for delivery drones: A comparison and assessment. *Transportation Research Part D: Transport and Environment*, *90*(December 2020).